MICRO-RAMAN MAPPING OF RESIDUAL STRESSES AT GRAIN BOUNDARIES IN MULTICRYSTALLINE BLOCK CAST SILICON SOLAR CELL MATERIAL: THEIR RELATION TO THE GRAIN BOUNDARY MICROSTRUCTURE AND RECOMBINATION ACTIVITY

G. Sarau*, M. Becker, and S. Christiansen
Institute of Photonic Technology, Albert-Einstein Str. 9, D-07745 Jena, Germany
Max-Planck-Institute of Microstructure Physics, Weinberg 2, D-06120 Halle, Germany
M. Holla and W. Seifert
IHP/BTU Joint Lab, Konrad-Wachsmann-Alle 1, D-03013 Cottbus, Germany
*Correspondence: Tel: +49 3641 206401, Fax: +49 3641 206499, E-mail: george.sarau@ipht-jena.de

ABSTRACT: We study multicrystalline silicon (mc-Si) block cast wafer solar cell material with respect to mechanical residual stresses at grain boundaries (GBs) related to GB type, details of microstructure, and electrical activity of the GBs. For this purpose we combine micro-Raman spectroscopy, electron backscatter diffraction, and electron beam induced current techniques. Stresses of several tens of MPa are found not to influence the electrical activity in block cast mc-Si. Inhomogeneous distributions of residual stresses and electrical activity are observed along the same GB as well as along different GBs of the same type. These results are discussed in terms of local variations in the GB microstructure due to the presence of dislocations superimposed on the GB, their arrangement, intrinsic structure, and impurity decoration.
Keywords: Stress, Raman, Multicrystalline Silicon, Grain Boundary, Dislocation, Electrical Activity.

1 INTRODUCTION

In view of the ongoing decrease in wafer thicknesses in silicon solar cell production to reduce production costs, mechanical residual stresses produced during crystal growth and solidification as well as during wafer/cell processing are considered to belong to the main impediments to improve process yields [1, 2]. Thermal stresses resulting from inhomogeneous temperature gradients within the ingot during the block casting process that involves melting silicon and its solidification can partially or totally be relaxed by the formation of extended lattice defects such as dislocations, low-angle grain boundaries, cracks and their combinations. The remaining internal stresses alongside with an unfavourable configuration of structural defects may couple critically with external mechanical and thermal stresses during wafer sawing, solar cell and module production and handling leading to additional defects and unpredictable breakage of silicon wafers/cells [3]. Frequently, these stress-related defects act as recombination sites for minority carriers reducing the efficiency of solar cells [4, 5]. In this context, it is clear that understanding the stress states and their relations to microstructure and recombination activity of extended defects are of fundamental technological importance for multicrystalline silicon based solar cell technology.

While the infrared light transmission based techniques have a spatial resolution close to 100 µm and only the existence of stresses in arbitrarily oriented grains or the average shear stresses can be detected or estimated [4, 6], micro- Raman spectroscopy (µRS) can provide a lateral resolution better than 1 µm [7] and the determination of several stress tensor components within grains of arbitrary orientation [8, 9]. Recently, we have contributed some results [8, 9] to the ongoing discussion [1, 2, 3] on the origin of mechanical residual stresses in mc-Si. We have confirmed by µRS the presence of inhomogeneous residual stress distributions including local maximum compressive and tensile stresses in mc-Si at critical positions in terms of mechanical stability of the wafer/cell such as a highly defective area within a grain, a grain boundary accompanied by dislocations and a grain boundary triple point [9]. Since the control of GBs is considered to be among the main keys for improving the efficiency and mechanical stability of mc-Si solar cells [4, 5], in this study, we investigate the relation between residual stresses localized at GBs and the type, microstructure as well as electrical activity of the same GBs.

2 EXPERIMENTAL DETAILS

Commercially available p-type block-cast mc-Si solar cell material has been used in this study. Before the measurements, the sample (rectangular piece of 2 cm x 2 cm cut from an entire solar cell wafer) has been mechanically polished to remove the silicon nitride antireflective layer and to flatten the surface, followed by Secco-etching [10] for 5 seconds to reveal grain boundaries and dislocations. The Raman stress measurements were carried out at room temperature in the backscattering geometry using a LabRam HR800 spectrometer (from Horiba Jobin Yvon) equipped with a He-Ne laser with an excitation wavelength of 633 nm. The incident laser light was focused onto the sample's surface through a 100x objective (numerical aperture 0.9) resulting in a focused spot with a diameter of ~ 1 µm and a penetration depth of a few µm in silicon. The incident laser power under the microscope objective was ~ 2.3mW. The exposure time was 200 ms per spectrum. No shift due to the local heating of the sample by the laser beam was observed. The effect of the thermal instability of the laser and/or the Raman instrument on the silicon peak position was corrected by using one of the plasma lines of a Ne lamp located in the vicinity of the spectrometer's entrance hole [11, 12]. Several stress-tensor components can be determined by controlling the polarization direction of the incident and scattered light, taking into account the crystallographic orientations of the investigated grains:

$$\sigma = \begin{pmatrix} \sigma_{xx} & \tau_{xy} & 0 \\ \tau_{xy} & \sigma_{yy} & 0 \\ 0 & 0 & \Delta_z \end{pmatrix}$$

where the component Δ_z includes the stress components σ_{zz}, τ_{xz} and τ_{yz}. The polarized μ-Raman procedure is described in detail in Ref. [8].

To locate the GBs even in the Raman stress maps that display residual stresses rather than material topography, we have used the Raman intensity maps (not shown) where the grains can be well distinguished due to their different Raman scattering efficiency caused by their different crystallographic orientation with respect to the polarization of the incident light [9]. Thus, it is possible to relate grains and GBs to stress distributions by superimposing intensity and stress maps. The color coded bars below the stress maps measured with polarization settings for incident and scattered light are shown to give an idea about the Raman frequency shifts involved.

The grain orientation and grain boundary type were determined using an electron backscatter diffraction (EBSD) system from EDAX attached to a TESCAN LYRA XMU scanning electron microscope (SEM). The crystal orientation is described using the {hkl}<uvw> representation where {hkl} is the crystal plane perpendicular to the sample normal direction (z axis) and <uvw> is the crystal direction aligned with the transverse direction of the sample (y axis) [see Figs. 1 and 3 (d)]. The inverse pole figure (unit triangle) shows the sample normal direction relative to the axes of the measured crystal. The misorientation between adjacent grains is described using the angle/axis notation, that is, the rotation angle about the axis common to both lattices to bring them into coincidence, and in terms of Σ-value which denotes the fraction of atoms in the GB plane coincident in both adjacent lattices [13].

Prior to the electrical characterization by electron beam induced current (EBIC) technique, the sample was chemically polished in 1 HF: 2 HNO_3: 1 $C_2H_4O_2$ solution for 5 seconds. A 30 nm thick Al layer as Schottky contact was evaporated onto the sample surface, while the back ohmic contact was prepared by rubbing InGa alloy homogeneously over the back side of the sample. The EBIC measurements were taken with an EVO 40 SEM at 20 kV. The EBIC contrast used to evaluate the recombination strength was defined as $C=(I_{max}-I_{x,y})/I_{max}$, where I_{max} is the maximum EBIC current and $I_{x,y}$ are the EBIC currents at each measurement point. This definition provides EBIC contrast maps where the recombination activity of defects can be well spatially resolved when colorful scales are used [see Figs. 1-3 (b, c)].

3 RESULTS

The Raman stress map in Fig. 1(a) shows localized and quite symmetric stresses including both compressive (red area) and tensile (blue area) contributions close to a point denoted K, where Σ27a GB changes its direction. Virtually no stresses above and below this region as well as around the other GBs are observed. The Σ27a GB, described by a misorientation angle/axis of 31.59°/[110], changes its character to a large-angle random GB {38.2°/[315]} as well as its trajectory, when Σ3 GBs {60°/[111]} intersect it as displayed in the EBSD map in Fig. 1(d). The focused ion beam (FIB) marker allowed exact correlation between different measurement techniques. The localized stress distribution and its decay length resemble the stress field of an edge dislocation [14, 15] which, in our case, is superimposed on the GB.

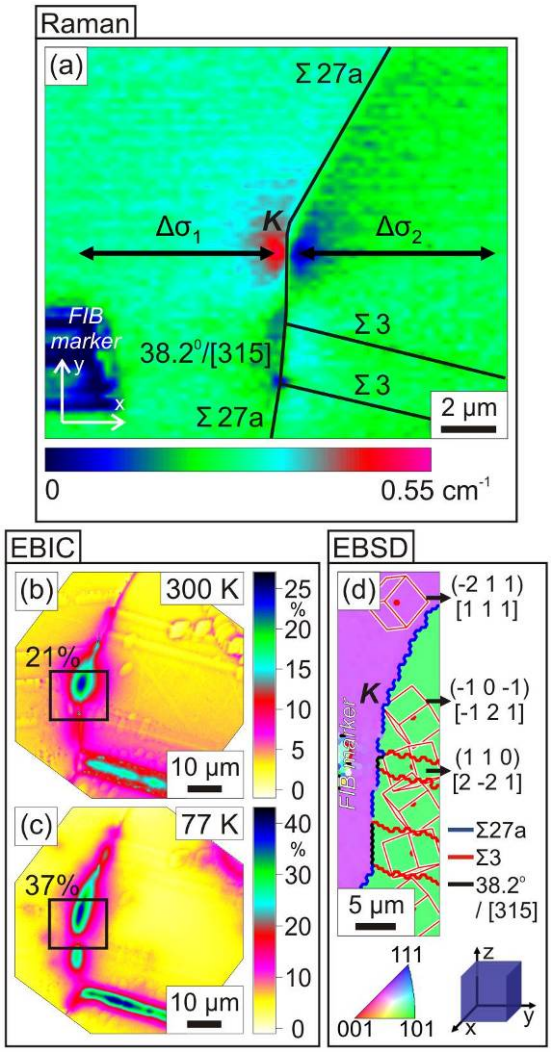

Figure 1: (a) Micro-Raman residual stress mapping of Σ27a, Σ3 and large-angle random {38.2°/[315]} GBs in block cast mc-Si. The investigated GBs show nearly no stresses around them except the localized compressive ($\Delta\sigma_1$) and tensile ($\Delta\sigma_2$) stresses close to a change in the Σ27a GB trajectory denoted K which are attributed to an edge dislocation superimposing the GB. (b, c) EBIC contrast images taken at 300K and 77K, respectively where the area enclosed by the rectangle represents the Raman mapped area displayed in (a). The numbers indicate the maximum contrast within the rectangles. The stressed area close to the Σ27a GB direction change and the stress-free area around it show similar EBIC contrasts. (d) EBSD map showing the grain orientations and GB types along with the orientation triangle and the sample reference frame.

The polarized μ-Raman stress measurements resulted in the following difference stress tensors referring to the coordinate system shown in Fig. 1(a). They have been evaluated between stressed positions close to the GB and positions at a distance from the GB which are not affected by the dislocation stress field:

$$\Delta\sigma_1 = \begin{pmatrix} -40\pm10 & -14\pm3 & 0 \\ -14\pm3 & -38\pm10 & 0 \\ 0 & 0 & -25\pm10 \end{pmatrix} MPa,$$

$$\Delta\sigma_2 = \begin{pmatrix} 33\pm10 & -7\pm1 & 0 \\ -7\pm1 & 31\pm10 & 0 \\ 0 & 0 & 34\pm10 \end{pmatrix} MPa.$$

The EBIC contrast images in Fig. 1(b) and (c) show strong contrasts (reduced minority carrier lifetime) of 21% at 300K and 37% at 77K in the region of the GB trajectory change and a contrast variation along the Σ27a GB. The region enclosed by the rectangle corresponds to the stress map in Fig. 1(a). By comparing the stress and EBIC images, it can be seen that the stressed area close to the change in the Σ27a GB trajectory denoted K and the stress-free area above and below it show similar EBIC contrasts, and thus similar recombination activities.

Figure 2(a) shows a Raman stress map of the same Σ27a GB at a distance of several millimeters from the position displayed in Fig. 1(a). The compressive (red area) and tensile (blue area) stresses are more extended along the GB, less symmetric, and change positions with respect to the GB as compared with the stress map in Fig. 1(a). This stress distribution is attributed to the stress field of an array of edge dislocations superimposing the GB [15]. The band-like less compressed region on the right-hand side of the Σ27a GB can be explained by the presence of dislocations (edge, screw and/or mixed), in the grain and close to the GB, which have locally rearranged to reduce the strain energy and thus, the stresses in this region [15]. The following stress-tensor gradients referring to the coordinate system shown in Fig. 2(a) have been determined by polarized μ-Raman:

$$\Delta\sigma_3 = \begin{pmatrix} 29\pm10 & -7\pm1 & 0 \\ -7\pm1 & 28\pm10 & 0 \\ 0 & 0 & 36\pm10 \end{pmatrix} MPa,$$

$$\Delta\sigma_4 = \begin{pmatrix} -34\pm10 & -3\pm1 & 0 \\ -3\pm1 & -37\pm10 & 0 \\ 0 & 0 & -37\pm10 \end{pmatrix} MPa.$$

Like in the previous case the stressed and stress-free areas around the GB in Fig. 2(a) are located in a region of similar (strong) EBIC contrast of 30% at 300K and 40% at 77K as indicated in Fig. 2(b) and (c), respectively and the recombination activity is inhomogeneous along the Σ27a GB.

Figure 3(a) shows two Σ9 GBs whose stress states are different, presumably, due to different arrangements of dislocations at the GBs. While the nearly horizontal Σ9 GB is stress-free, the vertical Σ9 GB show compressive (red area) and tensile (blue area) stresses unevenly distributed around it. The compressive and tensile stresses close to the middle of the vertical Σ9 GB are associated with an edge dislocation superimposed on the GB.

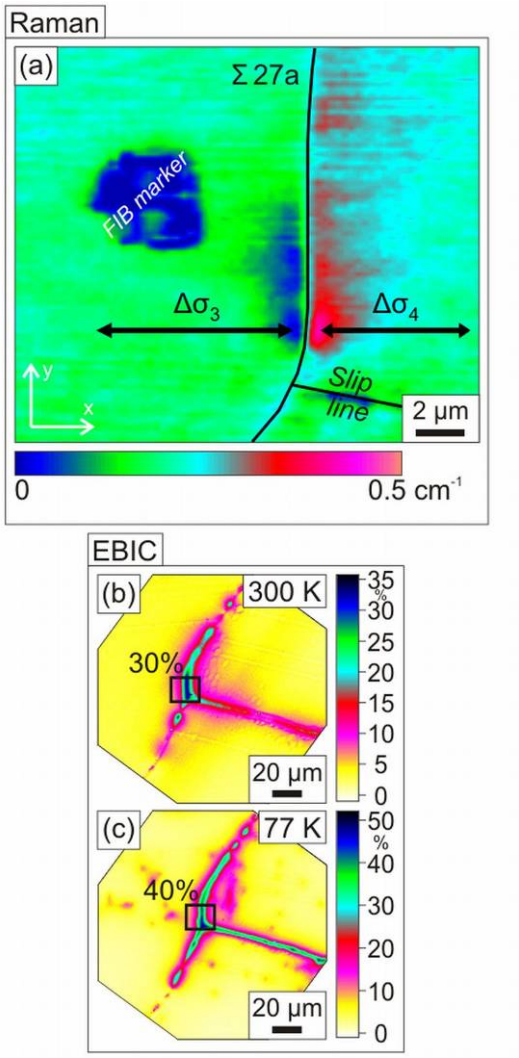

Figure 2: (a) Micro-Raman residual stress mapping of the same Σ27a GB at a distance of several millimeters from the position displayed in Fig. 1(a) showing a different stress distribution which is attributed to the stress field of an array of edge dislocations superimposed on the GB. (b, c) EBIC contrast images taken at 300K and 77K, respectively. The rectangle marks the Raman mapped area displayed in (a). The numbers indicate the maximum contrast within the rectangles. The stressed and stress-free areas along the Σ27a GB exhibit similar EBIC contrasts.

The other GBs exhibit almost no stresses around them. Stress measurements using polarized μ-Raman revealed the following stress-tensor gradients referring to the coordinate system shown in Fig. 3(a):

$$\Delta\sigma_5 = \begin{pmatrix} -30\pm9 & 3\pm1 & 0 \\ 3\pm1 & -27\pm13 & 0 \\ 0 & 0 & -28\pm9 \end{pmatrix} MPa,$$

$$\Delta\sigma_6 = \begin{pmatrix} 24\pm10 & 4\pm1 & 0 \\ 4\pm1 & 34\pm10 & 0 \\ 0 & 0 & 21\pm10 \end{pmatrix} MPa.$$

The electrical activities of the stressed and stress-free Σ9 GBs are weak at 300K (5% and 9%) and increase at 77K to 13% and 14%, respectively [see Fig. 3(b) and (c)].

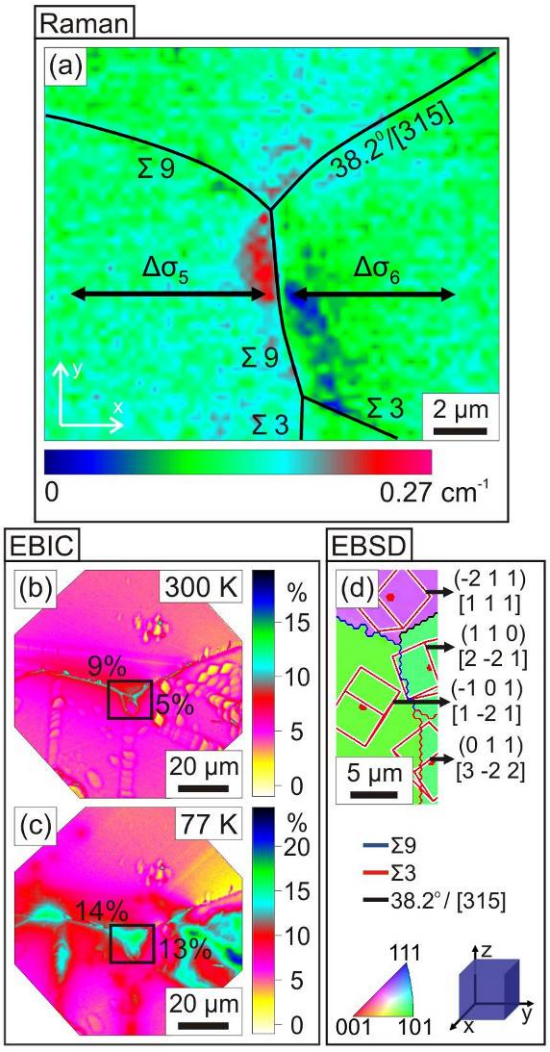

Figure 3: (a) Micro-Raman residual stress mapping of Σ9, Σ3 and large-angle random {38.2°/[315]} GBs in block cast mc-Si. Two Σ9 GBs showing different stress states attributed to particular arrangements of dislocations at the GBs are visible. (b, c) EBIC contrast images taken at 300K and 77K, respectively. The rectangle corresponds to the Raman mapped area displayed in (a). The numbers indicate the maximum contrast within the rectangles. The two Σ9 GBs show similar EBIC contrasts. (d) EBSD map showing the grain orientations and GB types along with the orientation triangle and the sample reference frame.

4 DISCUSSIONS

In addition to clean or metallic decorated dislocations superimposed on GBs which are extensively invoked in the literature to explain the EBIC contrasts along GBs [5, 16, 17], GB irregularities such as boundary steps also show recombination activity, namely, a dot-like EBIC contrast [18]. Since the measured EBIC contrasts are not dot-like and the Raman stress fields resemble those of edge dislocations as shown in Figs. 1-3 (a, b, c), our experimental results are discussed based on the presence of dislocations.

According to Shockley-Read-Hall theory [19], shallow levels in the band gap, e.g. those resulting from the strain fields of dislocations [16, 20, 21, 22], cause weak recombination activity of extended crystal defects at room temperature along with an increasing activity upon decrease of temperature. On the contrary, deep levels related to intrinsic core defects and/or metallic impurity decoration of dislocations result in a decrease of electrical activity for decreasing temperature [16, 17, 20, 21, 22]. We observed either quite strong (Fig. 1 and Fig. 2) or rather week EBIC contrast (Fig. 3) at room temperature, both increasing when decreasing temperature. Such type of temperature behaviour can be explained by the interaction of deep metal impurities or core defects at dislocations with shallow strain-field induced energy bands. The lower contrast of the defects in Fig. 3 indicates a smaller level of metal contamination or core defects [23].

Heterogeneous nucleation of dislocations takes place at regions of internal stress concentrations caused by local temperature and pressure gradients during crystal growth and solidification as well as during wafer/cell processing [15]. The local distribution of dislocations, their intrinsic structure and their impurity decoration are affected by many factors having a cumulative effect and resulting in an inhomogeneous and temperature dependent electrical activity as well as in a nonuniform distribution of the residual stresses. First, the nucleation, motion, multiplication and annihilation of dislocations under local thermal and mechanical stresses are dependent on the orientation, size and geometry of the grains as well as on the boundary conditions created by neighbouring grains [24, 25]. Since the two Σ9 GBs in Fig. 3(a) are formed between crystals of different orientations as shown by EBSD in Fig. 3(d), the different stress states at the two Σ9 GBs and the presence of one type of stresses along one side of the GB starting near the middle of the vertical Σ9 GB towards the two GB junctions can be explained by a different distribution of dislocations. Second, the GB interfaces must follow the growth direction and at the same time they must minimize their interfacial energy, namely the GB surface energy and the energy contribution from dislocations present at the GB [26]. Third, the strain energy of dislocations located either inside grains or on GBs is released by the local rearrangement in configurations in which the superimposed long-range stress fields of the dislocations cancel partially or totally [15].

Stressed and stress-free areas both showing similar electrical activity attributed to dislocations and their impurity decoration have been found around GBs as well as along different GBs of the same type confirming that only a particular arrangement of recombination active dislocations on GBs leads to stresses. These results can be taken as evidence that stresses of the order of several tens of MPa do not influence the electrical activity in block cast mc-Si. Indeed, comparably high stresses of up to 1.2 GPa in strained silicon as a transistor channel have been estimated to enhance the carrier mobility through the effective mass reduction and the band structure modification [27]. Such stress levels are also expected to influence the energy levels responsible for recombination activity in the case of mc-Si.

It is also interesting to discuss the stress distributions and stress tensors attributed to edge dislocations on GBs. Because of the finite laser spot diameter, the Raman signal in the center of an edge dislocation consists of shifts to higher and lower frequencies corresponding to compressive stresses above the slip plane and tensile stresses below the slip plane, respectively. This results in spectra frequency shifts at the GBs containing the dislocation center which are nearly similar to those at stress-free positions inside grains and in a broadening of the spectra's full width at half maximum - FWHM (not shown). Thus, μRS can not provide the maximum stress located at the dislocation core but rather the stress averaged over ~ 1 μm diameter spot when probing inside grains close to the GB containing the dislocation core. The different values of identical stress tensor components describing the compressive or tensile part of the edge dislocations can be explained by their different intrinsic structure and/or by the different accumulation and distribution of impurity atoms in form of submicron precipitates in the dislocation cores or in the strain fields of dislocations [16]. However, the probability of a mixed dislocation having the stress field of the edge component predominant over that of the screw component can not be fully ruled out.

5 CONCLUSIONS

The relation between mechanical residual stresses at GBs in block cast mc-Si and the GB type, microstructure and electrical activity has been studied using micro-Raman spectroscopy, EBSD and EBIC. Our experimental results show that the distributions of residual stresses and electrical activity are inhomogeneous along the same GB as well as along different GBs of the same type. These non-uniformities are considered to be caused by local variations in the GB microstructure mainly attributed to the presence of dislocations, their intrinsic structure, impurity decoration and arrangement on GBs. The values of the stress tensor components determined at edge dislocations superimposing the GBs are too small, i.e. several tens of MPa, to influence the electrical activity. Therefore, the existence of both stressed and stress-free areas exhibiting similar electrical activities at GBs is explained by a particular arrangement of recombination active dislocations at GBs. Our study demonstrates that micro-Raman spectroscopy can be used to identify experimentally the defect type by comparing its stress field distribution and its stress tensor components with theoretical calculations.

6 ACKNOWLEDGMENTS

This work was financially supported by the German Federal Ministry for the Environment, Nature Conservation and Nuclear Safety and all the industry partners within the research cluster SolarFocus (0327650 D + A) and by the Max-Planck Society within the project Nanostress. The content of this publication is the responsibility of the authors.

6 REFERENCES

[1] J. Gustafsson, H. Larsson, H. Jørgen Solheim, and T. Boström, In Proceedings of the 23rd European Photovoltaic Solar Energy Conference, Valencia, Spain (2008) p. 1957.
[2] X.F. Brun and S.N. Melkote, Sol. Energy Mater. Sol. Cells 93 (2009) 1238.
[3] P. J. Withers, Rep. Prog. Phys. 70 (2007) 2211.
[4] J. Chen, B. Chen, T. Sekiguchi, M. Fukuzawa, and M. Yamada, Appl. Phys. Lett. 93 (2008) 112105.
[5] J. Chen and T. Sekiguchi, Jpn. J. Appl. Phys. 46 (2007) 6489.
[6] S. He, S. Danyluk, I. Tarasov, and S. Ostapenko, Appl. Phys. Lett. 89 (2006) 111909.
[7] V. Poborchii, T. Tada, and T. Kanayama, Appl. Phys. Lett. 91 (2007) 241902.
[8] M. Becker, H. Scheel, S. Christiansen, and H. P. Strunk, J. Appl. Phys. 101 (2007) 063531.
[9] G. Sarau, M. Becker, G. Andrä, and S. Christiansen, In Proceedings of the 23rd EU PVSEC, Valencia, Spain (2008) p. 2265.
[10] F. Secco D' Aragona, J. Electrochem. Soc. 119 (1972) 948.
[11] I. De Wolf, Sci. Technol. 11 (1996) 139.
[12] G. Sarau, M. Becker, A. Berger, J. Schneider, and S. Christiansen, Mater. Res. Soc. Symp. Proc. 1024E (2007) 1024-A07-04.
[13] H. Grimmer, W. Bollmann, and D. H. Warrington, Acta Crystallog. A30 (1974) 197.
[14] G. Irmer and M. Jurisch, phys. stat. sol. (a) 204 (2007) 2309.
[15] D. Hull and D. J. Bacon, Introduction to Dislocations, Butterworth-Heinemann (2001), Chapter 4 and 9.
[16] M. Seibt, R. Khalil, V. Kveder, and W. Schröter, Appl. Phys. A 96 (2009) 235.
[17] J. Chen, T. Sekiguchi, D. Yang, F. Yin, K. Kido and S. Tsurekawa, J. Appl. Phys. 96 (2004) 5490.
[18] Z.-J. Wang, S. Tsurekawa, K. Ikeda, T. Sekiguchi, and T. Watanabe, Interface Science 7 (1999) 197.
[19] W. Shockley and W. T. Read, Phys. Rev. 87 (1952) 835.
[20] Z. J. Radzimski, T. Q. Zhou, A. Buczkowski, G. A. Rozgonyi, D. Finn, L. G. Hellwig, and J. A. Ross, Appl. Phys. Lett. 60 (1992) 1096.
[21] M. Kittler, W. Seifert, and V. Higgs, phys. stat. sol. (a) 137 (1993) 327.
[22] S. Kusanagi, T. Sekiguchi, and K. Sumino, Appl. Phys. Lett. 61 (1992) 792.
[23] V. Kveder, M. Kittler, and W. Schröter, Phys. Rev. B 63 (2001) 115208.
[24] J. Cochard, S. Gouttebroze, S. Dumoulin, M. M'Hamdi, and Z. L. Zhang, In Proceedings of the 23rd European Photovoltaic Solar Energy Conference, Valencia, Spain (2008) p. 1919.
[25] S. Dumoulin, S. Gouttebroze, and M. M'Hamdi, In Proceedings of the 23rd European Photovoltaic Solar Energy Conference, Valencia, Spain (2008) p. 1924.
[26] K. C. Yoo, S. M. Johnson and W. F. Regnault, J. Appl. Phys. 57 (1985) 2258.
[27] J. Chung, G. Lian, and L. Rabenberg, Appl. Phys. Lett. 93 (2008) 081909.